Relative pK_a Values from First-Principles Molecular Dynamics: The Case of Histidine Deprotonation

Ivaylo Ivanov,*,† Bin Chen,‡ Simone Raugei,§ and Michael L. Klein†

Center for Molecular Modeling and Department of Chemistry, University of Pennsylvania, 231 South 34th Street, Philadelphia, Pennsylvania 19104-6323, Department of Chemistry, Louisiana State University, Baton Rouge, Louisiana 70803-1804, and International School for Advanced Studies and INFM Democritos Center, via Beirut 2-4, 34014 Trieste, Italy

Received: November 21, 2005; In Final Form: February 1, 2006

Accurate calculation of pK_a values and free energies for acid/base reactions in the condensed phase has been a long-standing goal of theoretical chemistry. We present a novel application of the Car−Parrinello molecular dynamics method to the problem of relative pK_a determination. As a particular example, we focus on the second stage in the dissociation of histidine, a process that holds special importance for biology. Using constrained molecular dynamics, we have analyzed the structural, electronic, and dynamical transformations taking place along a preselected, intuitive reaction coordinate. By integrating the potentials of mean force for the deprotonation of histidine and for a reference reaction, autodissociation of water, we obtain a pK_a value of 6.8, which appears to be in good agreement with the experimental estimate of 6.1. Detailed analysis was undertaken to determine the value of the constraint, which transformed the N*−H* from a covalent to a hydrogen bond. This helped to identify a number of properties that could be successfully used in monitoring the dissociation process. Additional analysis in terms of electron localization functions provided valuable insight into the nature of the deprotonation reaction.

1. Introduction

Weak acid ionization processes are commonplace throughout chemistry and biochemistry, and their importance has prompted considerable experimental and theoretical attention.[1−4] Recent ab initio molecular dynamics (AIMD) studies have provided valuable insight into the mechanisms of dissociative processes, most notably for the autodissociation of water.[5−7] However, due to certain technical difficulties, such as the use of very small periodic boxes and the inherent limitations of the commonly used exchange and correlation functionals, the free energy difference between the bound and the charge-separated state was underestimated.[5] Relating the free energies from those studies to pK_a values is further complicated by the fact that the calculated potentials of mean force (PMFs) are relative and do not correspond to infinite separation between the products of the reaction. The resulting uncertainty in the free energy practically precludes their use to determine absolute pK_a values. In view of the above, for the present work we found it advantageous to focus on calculating relative pK_a values instead. Herein, we present the results of an extensive first-principles investigation of the second stage in the dissociation of histidine. The main focus of our work is on developing a robust procedure to calculate relative pK_a values based on first-principles molecular dynamics.[8] To this end, we have determined potentials of mean force (PMFs) for the dissociation reaction and explored their relation to pK_a. We have settled on an approach commonly used in calculating covalent binding constants wherein the binding constant is defined as the integral of the Boltzmann factor over the potential of mean force for the two ions[1]. From the ratio of two such integrals, one for the reaction in question and another for a reference reaction, a K_a value can be determined provided that the equilibrium constant for the reference reaction is known, thus alleviating the systematic underestimation arising from finite size effects and from deficiencies of the density functional theory (DFT) functional. Since weak acid ionization is a reaction strongly influenced by solvent reorganization,[10] the explicit inclusion of the solvent is crucial. A distinctive feature of the AIMD approach is the explicit treatment of all solvent molecules at the same ab initio level of theory as the solute system. This helps account for many-body and polarization effects not normally included in classical molecular dynamics simulations. As an important test case we have investigated the deprotonation of L-histidine. The paper is organized as follows: (i) computational details are included in section 2; (ii) section 3.1 provides methodological details regarding constrained dynamics, the blue moon ensemble method, and the statistical mechanical expression for calculating relative pK_a values; (iii) section 3.2 elaborates on our results with special emphasis on the calculated PMFs; in section 3.3 we outline a number of properties that can be used to monitor the bond-breaking process and define the range of the control parameter ξ, which preserves covalent bonding between the N* atom and its adjacent H atom; (iv) finally, section 4 contains our conclusions and directions for future work.

2. Methods and Simulation Details

Car−Parrinello molecular dynamics simulations have been carried out on L-histidine. The system consisted of 1 histidine molecule plus 49 water molecules contained in a periodically replicated cubic box of dimensions 11.74 × 11.74 × 11.74 Å.

* Author to whom correspondence should be addressed. Present address: Department of Chemistry and Biochemistry, University of California-San Diego, Urey Hall M/C 0365, 9500 Gilman Drive, La Jolla, CA 92093-0365. E-mail: iivanov@mccammon.ucsd.edu.

† University of Pennsylvania.

‡ Louisiana State University.

§ International School for Advanced Studies and INFM Democritos Center.

10.1021/jp056750i CCC: $33.50
Published on Web 03/08/2006

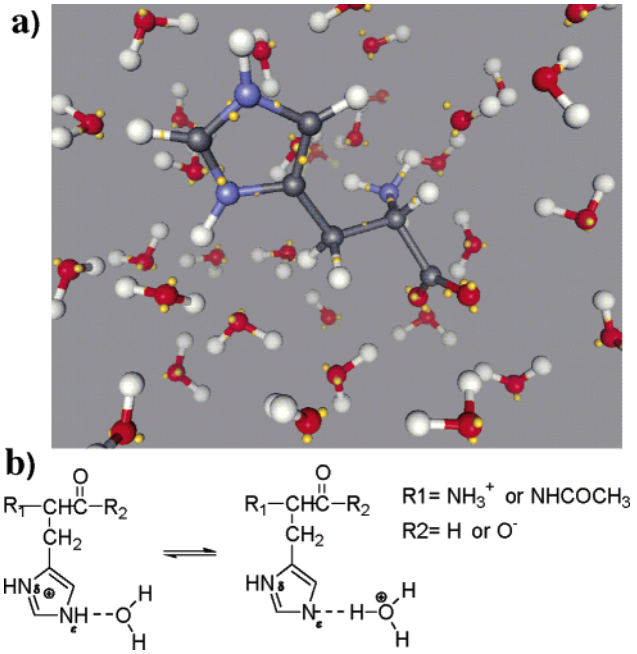

Figure 1. (a) Snapshot of a typical configuration from an unconstrained dynamics trajectory. The hydrogen, carbon, oxygen, and nitrogen atoms are color-coded in white, gray, red, and blue; the positions of the Wannier function centers (centers of charge of localized molecular orbitals,[9] indicative of the bonding pattern, are shown in gold. (b) Schematic representation of the deprotonation reaction.

A snapshot of a typical configuration and a schematic representation of the histidine dissociation reaction are shown in Figures 1a and 1b, respectively. For the reference reaction, water autodissociation, we used a system containing 32 water molecules in a cubic box of 9.86 × 9.86 × 9.86 Å with periodic boundary conditions. The size of the systems considered is sufficient to provide the complete first and second solvation shells of the solute (either a histidine or a water molecule) plus part of the third shell. This fact makes comparison between the two systems fully meaningful. All simulations were performed with the program CPMD.[11] The gradient-corrected HCTH[12,13] functional was adopted. In addition to providing good structural description of aqueous systems, this functional yields improved energetics compared to the popular BLYP[14,15] functional, specifically for hydrogen abstraction reactions in the gas phase.[12] The core electrons were accounted for in our simulations by nonlocal norm-conserving pseudopotentials of the Troullier−Martins[16] type. For the heavy atoms these have been transformed to a fully nonlocal form using the scheme of Kleinman and Bylander.[17] The valence electronic wave functions were expanded in a plane wave basis set with an energy cutoff of 70 Ry. Hydrogen nuclei were treated as classical particles with the mass of the deuterium isotope. Thus, the nuclear quantum effects were not included in our simulation. Nevertheless, quantum effects might be significantly manifested for this reaction. The difference between the zero point energies (ΔZPE) associated with imidazolium ion deprotonation and the reference water autodissociation reaction can serve as an estimate for the magnitude of these effects and their influence on the calculated free energies. In this respect, the advantage of calculating relative pK_a values becomes apparent: By selecting a reference reaction, for which the ZPE contribution is expected to be comparable, we can minimize the influence of the nuclear quantum effects on the results. In our case, the calculated ΔΔZPE (Table 1 of the Supporting Information) of −0.46 kcal mol^{-1} corresponds to a shift in the estimated pK_a of −0.34 units and is considerably below the inherent accuracy of the DFT functional. To fully account for nuclear quantum effects (including tunneling) one has to carry out expensive path integral simulations, which are beyond the scope of the current work. A fictitious mass of 800 au was ascribed to the electronic degrees of freedom consistent with the recommended $\sim 1/5$ of the mass of deuterium isotope.[18,19] This choice allowed the equations of motion for the atomic nuclei to be propagated with a time step of 0.15 fs. The adiabatic separation of the nuclear and electronic subsystems is fully preserved along all AIMD trajectories. The simulations were performed in the NVT ensemble, and the temperature was maintained at ∼300 K by the use of a Nosé−Hoover chain of thermostats[20,21] with a chain length of four and a target frequency of 500 cm^{-1}. This set of parameters enabled us to maintain adiabatic conditions for the electrons over the full length of the trajectories.

3. Results and Discussion

3.1. Potentials of Mean Force. Weak acid dissociation is a rare event on the time scale of ab initio molecular dynamics and thus not accessible through direct simulations. Constrained molecular dynamics can circumvent this difficulty and enforce dissociation, through the use of a control parameter ξ, typically chosen to resemble the respective reaction coordinate, whose values are held constant and then varied in increments throughout the simulation.[22−24] When the underlying potential energy surface is inherently complex in multiple dimensions, as is often the case for condensed phase reactions, the use of simple geometric constraints can be a rather poor approximation to the true reaction coordinate and can lead to problems, especially in attempts to locate transition states.[23] Nevertheless, geometric constraints that distinguish unambiguously between reactant and product states can still be utilized to determine free energy differences.[23,24] This is due to the fact that the Helmholtz free energy is a function of state and, thus, independent of the exact reversible path used to connect the initial and final states. Both simple linear[5,6] and collective[7] (e.g., coordination) constraints have been applied to the problem of water autodissociation. The advantage of the latter lies in the ability to control the coordination of a species (protonation state in the case of hydrogen coordination) without the need to specify distances to particular hydrogen atoms. This, in turn, prevents ion recombination that would normally occur with linear constraints at the end of the PMF due to proton transfer. In our present investigation we have relied on linear constraints, primarily for their simplicity. In particular, the N*−H distance between one of the imidazole nitrogens and its neighboring hydrogen ($\xi = |r_{N^*} - r_H|$) was varied between 0.8 and 1.8 Å with an increment of 0.05 Å. For each constrained configuration we have obtained trajectories starting from well-equilibrated unconstrained configurations. After reequilibration for 1.0 ps the properties of interest were averaged for an additional 10 ps. The constraint was linearly added to the CP Lagrangian according to the blue moon ensemble method.[22,24] The method corrects for the bias in the statistics for momentum space due to the introduction of constraints in coordinate space. Within this method the relative free energy between states ξ_0 and ξ_1 can be evaluated using the expressions

$$\Delta F = -\int_{\xi_0}^{\xi_1} f_{\xi'} \mathrm{d}\xi' \quad f_{\xi'} = \frac{\langle Z^{-1/2}[\lambda - k_B T G]\rangle_{\xi'}}{\langle Z^{-1/2}\rangle_{\xi'}} \qquad (1)$$

where f_ξ is the average force of constraint, k_B is the Boltzmann constant, T is the temperature in Kelvin, and Z and G are weight

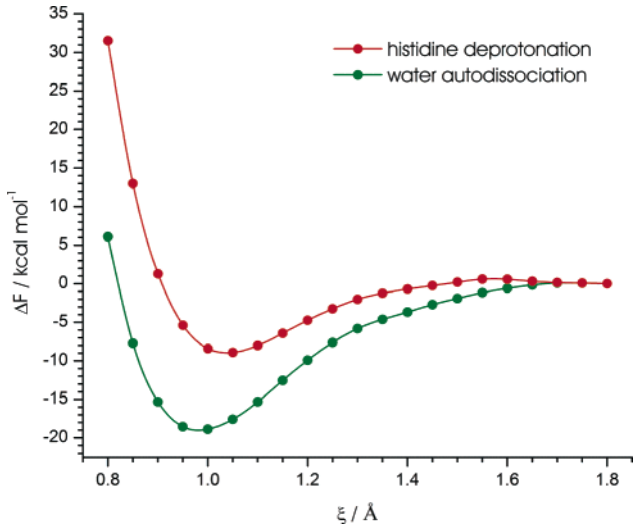

Figure 2. Potentials of mean force: (i) for the deprotonation of L-histidine from the Nϵ position (shown in red) and (ii) for water autodissociation (shown in green).

and correction factors associated with the transformation from generalized to Cartesian coordinates.[24] In the case of a distance constraint the second equation reduces to a simple ensemble average of the Lagrange multiplier λ: $f_{\xi'} = \langle\lambda\rangle_{\xi'}$.

The free energy profiles resulting from the above integration are plotted in Figure 2. The dissociation of histidine proceeds in several stages.[22] In summary, first the polar N*−H bond is extended harmonically; then the bond transformation (conversion of the N*−H bond from covalent to hydrogen) takes place from $\xi \approx 1.2$ to 1.35 Å; at 1.4 Å the proton is completely transferred to the O*, and therefore, the free energy curves level off after this point; from about $\xi \approx 1.5$ Å proton transfer attempts from the newly formed hydronium ion become possible; these are generally not successful until after the transition state (at separation $\xi \approx 1.6-1.65$ Å), when the constraint force changes its sign.

The pK_a value for a weak acid in aqueous solution can be related to the value of the Helmholtz free energy for the hydrogen abstraction reaction. Thus, the dissociation constant can be represented as follows[1,27]

$$K_c^{-1} = C_0 \int_0^\infty H(r)\, e^{-\beta w(r)} 4\pi r^2\, dr \quad H(r) = \begin{cases} 1 & r < R_c \\ 0 & r \geq R_c \end{cases} \quad (2)$$

where K_c is the equilibrium constant for dissociation (expressed in terms of concentration), C_0 is the standard concentration, $H(r)$ is a Heaviside function, $w(r) = \Delta F(r)$ is the potential of mean force, and R_c is a distance cutoff used to distinguish between the case of a covalently bonded and a dissociated H atom. The contribution in eq 2 from values of r below 0.8 Å is negligible due to the fact that the $w(r)$ term appears in the exponent and due to the steep increase in the PMF in that region. The above expression shows that direct estimation of the pK_a value from the energy difference at the two ends of the PMF can be problematic for two reasons. First, it ignores an entropic contribution from the bond-breaking process, leading to a missing volume-dependent term in the expression for K_a. Second, what is available from simulations are relative potentials of mean force, referred to a finite separation between the products. Therefore, absolute pK_a determination from these data is difficult. However, one may take advantage of the fact that from some distance on, after the transition state, the PMF becomes rather generic. (Namely, it corresponds to two ions being separated further and further in solution.) This opens up the possibility that the determination of relative pK_a values may be less error prone. By taking the ratio of dissociation constants for the reaction under consideration and a reference reaction, according to eq 2 we obtain

$$\frac{K_d(\mathrm{His})}{K_d(\mathrm{H_2O})} = \frac{\int_0^{R_c} e^{-\beta w_{\mathrm{H2O}}(r)} r^2\, dr}{\int_0^{R_c} e^{-\beta w_{\mathrm{His}}(r)} r^2\, dr} \quad (3)$$

3.2. pK_a and Statistical Accuracy. Potentials of mean force that begin at the equilibrium N−H bond length, corresponding to the free energy minimum for the covalent N−H bond may serve as a reasonable basis for comparison between the tautomeric forms of histidine and a capped analog.[22] However, for the purposes of calculating relative pK_a values they need to be extended both in the direction of shortening as well as lengthening of the N−H bond (Figure 2). The length of our PMF is limited by the onset of proton transfer toward the end of the simulation. For large values of ξ this process renders a linear constraint ineffective in enforcing the desired reaction coordinate and prevents further extension of the PMF.

We have used a rigorous approach, stemming from statistical mechanics, to calculate the ratio of equilibrium constants for the deprotonation of histidine and for a reference reaction (water autodissociation), which takes into account the aforementioned entropic contribution. By integrating the potentials of mean force according to eq 3 and setting the cutoff radius R_c to 1.35 Å (for details, see section 3.3) we obtain a pK_a estimate of 6.8. This appears to be in good agreement with the experimental value of 6.1. Closer agreement is not to be expected, given the present level of accuracy of the DFT functionals, the statistical uncertainty associated with thermodynamic integration, and the fact that contributions from ΔZPE and possible quantum tunneling of the proton (see remarks at the end of section 2) are neglected. Since the dissociation constant K is related to the free energy difference through an exponential relationship small errors in the ΔF term can lead to relatively large deviations in K_a. Nevertheless, as we have shown, this approach is sufficiently robust to provide useful estimates of pK_a and free energy differences. It is expected to be applicable to systems much more complicated than the test case of histidine.

A few comments are in order regarding the convergence of the results. The typical length of the constrained trajectories in our study (after equilibration) has reached 10 ps. This amounts to 10 times longer sampling compared to all previous constrained AIMD studies. During this time the constraint forces and correspondingly the points of the PMF can be converged with very small statistical uncertainties. (Figure 3 depicts the running average of the calculated constraint force for typical trajectories.) While this fact does not completely preclude the possibility of systematic deviations, which may occur at longer times, the solvent degrees of freedom are adequately sampled in our simulations (including the fast intramolecular vibrations, rotational motion, librations, and even the more large-scale collective motions of the water molecules). Most importantly, substantial reorganization of the hydrogen bond network around the solute is seen on this time scale. Hydrogen bond rearrangement has been put forth as an important contribution of the solvent toward stabilizing the products of the dissociation.[28] It should also be mentioned that AIMD has an inherent advantage in terms of sampling when compared to classical molecular dynamics for reactions involving separation of charge. In that case, the instantaneous response of the solvent electronic degrees

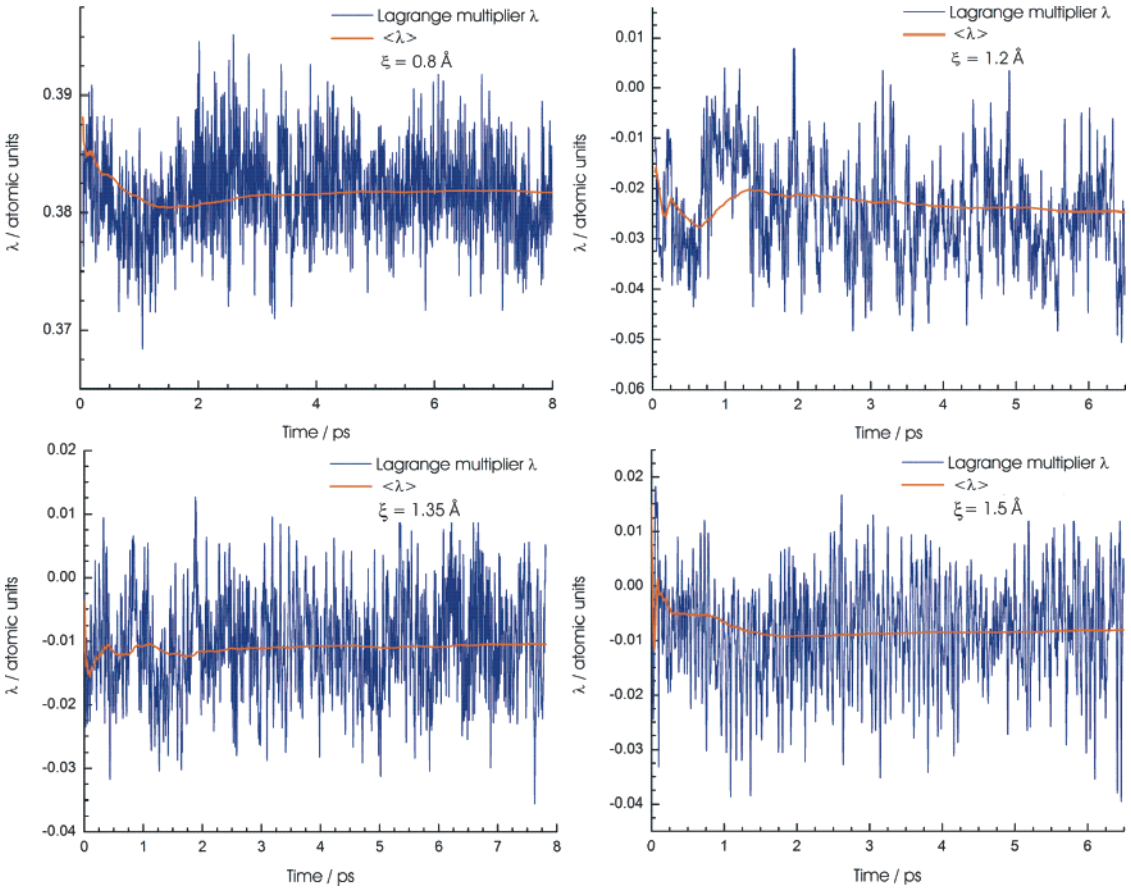

Figure 3. Instantaneous value and average of the Lagrange multiplier λ for several constrained dynamics trajectories with different values of ξ.

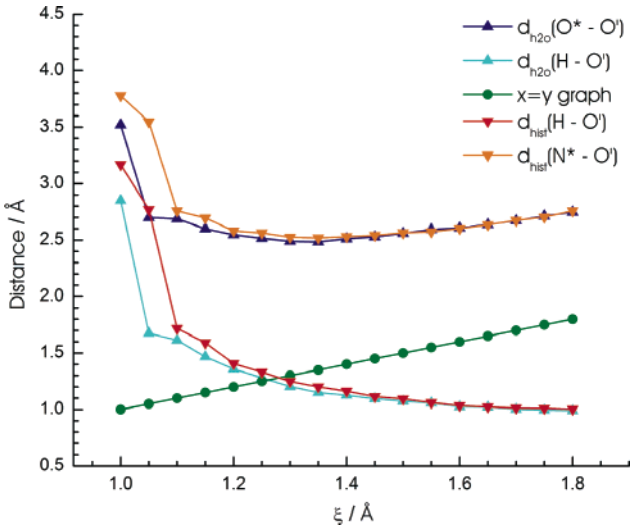

Figure 4. Average bond distances as a function of the control parameter ξ. Shown are the d_{H_2O}(H−O′) and d_{H_2O}(O*−O′) distances for the case of water autodissociation and d_{His}(H−O′) and d_{His}(N*−O′) distances for the case of histidine deprotonation.

of freedom to the changing charge distribution on the solute is automatically included, whereas classical molecular dynamics cannot account for this effect. Therefore, it has to rely on purely geometric reorientation of the solvent to stabilize the solute. The cumulative length of our simulation trajectories substantially exceeded half a nanosecond. Such extensive sampling is to our knowledge unprecedented for constrained AIMD dynamics in an aqueous system.

3.3. Structural Electronic and Dynamical Properties. We have examined the ensemble-averaged structural properties for different values of the distance constraint ξ to determine a suitable value for the cutoff radius R_c appearing in eqs 2 and 3. Figure 4 depicts the average H−O′ and N*−O′ distances as a function of the control parameter ξ. The N*−H distance ($y = x$ line) is also shown for completeness. The corresponding distances for water autodissociation (O*−H, H−O′, and O*−O′) are displayed on the same graph to allow for comparison. In both cases, when the constraint value is increased the H−O′ distance smoothly decreases until it reaches the average value of an OH bond in a hydronium ion (for $\xi \geq 1.4$ Å). The point where the N*−H and H−O′ curves intersect can be regarded as a reasonable approximation for the cutoff radius R_c. This finding is further reinforced by the position of the minimum in the N*−O′ and the O*−O′ curves, which also occurs at $\xi \approx$ 1.3/1.35 Å and reflects the well-established fact that the distance between the heavy atoms participating in proton transfer contracts during the reactive event.

A unique advantage of AIMD is that it allows a detailed microscopic analysis of bond breaking and formation from the point of view of quantum chemistry. In particular, the electron localization function (ELF) of Becke and Edgecombe[29,30] is a convenient tool for monitoring the bond-breaking process

$$\mathrm{ELF} = (1/(1+\chi)^2) \qquad \chi = \frac{\frac{1}{2}\sum_i |\nabla\Psi_i|^2 - \frac{1}{8}\frac{(\nabla\rho)^2}{\rho}}{C_F\rho^{5/3}} \quad (4)$$

Here ρ denotes the electron density, C_F is the Fermi constant, $C_F = {}^3/_{10}(3\pi^2)^{2/3}$, and ψ_i are the doubly occupied Kohn−Sham orbitals in a spin-restricted DFT calculation.

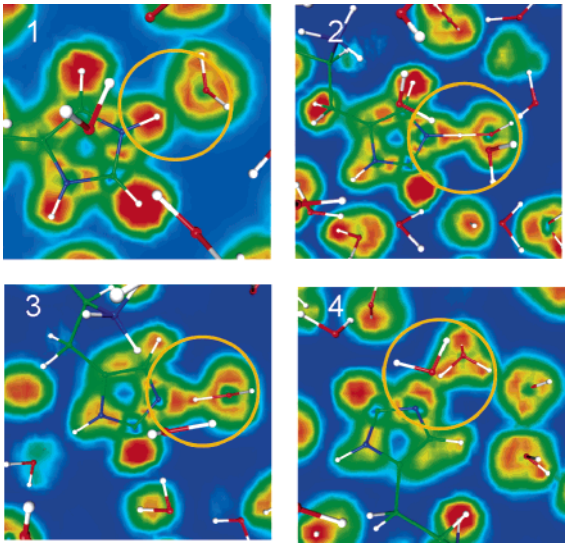

Figure 5. Contour plots of the electron localization function (ELF) for four values of ξ: (1) 1.1, (2) 1.3, (3) 1.35, and (4) 1.5 Å. The N−H bond of interest is highlighted with a gold circle.

The ELF is defined as the inverse of the parameter χ, which represents the difference in the electronic kinetic energy density for the system with and without Pauli exclusion, normalized by the Thomas−Fermi energy term (the electronic kinetic energy density of the uniform electron gas). Along the reaction pathway ELF varies parametrically with the nuclear configuration, and the transformations in bonding are manifested in the appearance and disappearance of local maxima. Figure 5 depicts these transformations in ELF as the constraint is being varied. The formation of an intermediate structure at $\xi \approx 1.35$ Å denotes the breaking of the covalent bond between N* and H and its transformation into a hydrogen bond. Thus, the electron localization function can be identified as a convenient and sensitive criterion for determining the cutoff radius in eq 2. In addition to ELF, we also examined the usefulness of properties derived from population analysis[31] in monitoring the dissociation process. We calculated Mulliken and Löwdin charges from randomly chosen snapshots toward the end of each constrained trajectory and examined how they evolve as a function of the constrained reaction coordinate (shown in Figures 1 and 2 of the Supporting Information). Overall, they were not very indicative of the occurrence of dissociation and were not even monotonic, likely as a result of statistical uncertainty. In addition, they displayed all the deficiencies attributed to the use of different charge partitioning schemes. Only the Mayer bond orders[32] calculated from the Mulliken population analysis showed significant correlation with the other independent criteria in determining the bond transformation but, as shown in Figure 3 of the Supporting Information, tended to slightly overestimate the value of R_c to ~1.45 Å.

Finally, we have examined the possibility of monitoring the dissociation process by looking at changes in the dynamical response of the system and, more specifically, changes in the fluctuations of the constraint forces as a function of the bonding environment in the vicinity of the constrained atoms. The most direct dynamical information that can be obtained from our constrained trajectories is the autocorrelation function of the constrained force

$$C_{\xi}(t) = \langle f_{\xi}(\tau) f_{\xi}(t+\tau) \rangle \qquad (5)$$

Such functions, characteristic of dipole−dipole relaxation processes, have been shown previously[6] to be sensitive to the bonding environment around the distance constraint. We have, therefore, explored the possibility of using this function as a potential criterion for determining the value of the constraint ξ that leads to the termination of the covalent bond between N* and H. In Figures 6a and 6b we present a number of autocorrelation functions corresponding to different values of the distance constraint. It is evident that the overall decay rate

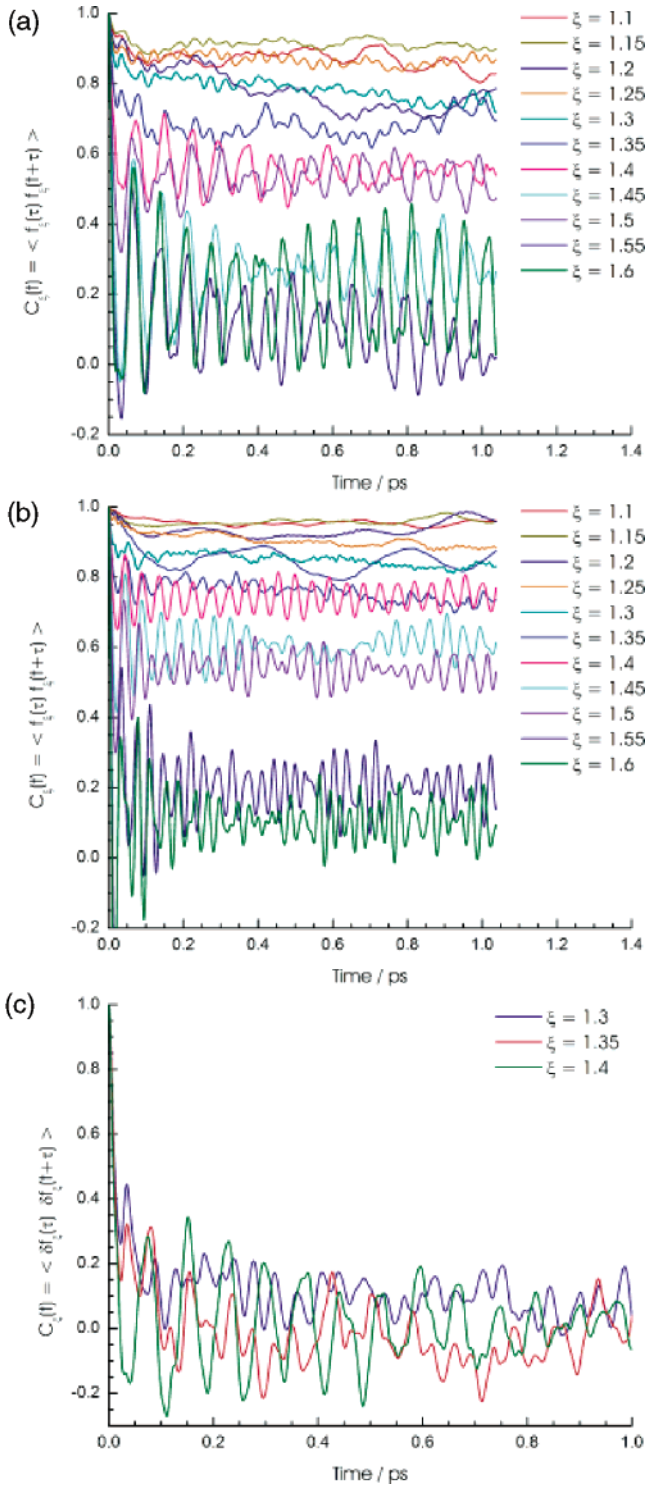

Figure 6. Constrained force autocorrelation functions for values of the control parameter ξ ranging from $\xi = 1.1$ to 1.6 Å in increments of 0.05 Å for (a) histidine deprotonation and (b) water autodissociation. Normalized autocorrelation functions of the fluctuations in the constraint force for $\xi = 1.3$, 1.35, and 1.4 Å are shown in part c.

and the oscillatory behavior of these functions changes qualitatively in the interval $\xi = 1.1$ Å to $\xi = 1.6$ Å. The initial decay rates are slower for low values of ξ, whereas in the case of large ξ, the decay rates are significantly faster and the oscillations more frequent and with larger amplitudes. To facilitate comparison, in Figure 6c we have plotted the normalized autocorrelation function of the fluctuations in the constraint force. Namely, we subtracted the average of the constrained force and looked at the magnitude of the deviations, so that the curves asymptotically go to zero rather than the square of the average force of constraint (as expected from the Onsager regression hypothesis). Then, we normalized the curves to start from unity, dividing them by the value of their first element. An intermediate behavior is displayed clearly at $\xi = 1.35$ Å for histidine deprotonation. The explanation for the character of the observed dynamical responses is that when the constraint is being enforced over a covalent bond the neighboring bond is a hydrogen bond and, thus, exhibits slower relaxation patterns. Conversely, when the deprotonation event has already occurred the constraint is enforced on a hydrogen bond, flanked by covalent bonds. These covalent bonds demonstrate much faster response and higher oscillation amplitudes. Our results demonstrate that the dynamical response of the environment around the constrained atoms is sensitive to the chemical transformation taking place in the system. In fact, the intermediate behavior at $\xi = 1.35$ Å correlates very well with our observations of bond breaking at that point based on structural and electronic criteria. It should also be noted that the use of a Nosé−Hoover thermostat could affect the autocorrelation function of the constrained force and lead to artificially fast relaxation. A frequency of the thermostat of 500 cm^{-1} (as the one used in our simulation) corresponds to a time period of 67 fs and could potentially affect the decay rates for $\xi \leq 1.3$ Å. In view of this fact, the thermostat was switched off for the entire range of constraint values shown in Figure 6, and the constrained trajectories were continued in the NVE ensemble for the purpose of calculating the $C_\xi(t)$ autocorrelation functions.

Toward the end of this section, in which we examined different ways of monitoring the bond conversion process, we should comment on the robustness of the results with respect to the choice of the cutoff radius R_c. It may appear from examining eqs 2 and 3 that finding an accurate value for R_c is critical for the precise determination of pK_a. However, the PMF can be related to a pair correlation function $g(r)$ for the two ions separated by a distance r in an equilibrium solvent[9]

$$w(r) = -k_B T \ln g(r) \tag{6}$$

This function has a gap between the first and second maximum corresponding to the maximum in the PMF that reflects the very small probability for the ions to reside at distances in the transition region. Furthermore, we observe that the steepest increase in the PMF occurs prior to the dissociation of the covalent bond. It should, therefore, be possible to select a cutoff radius anywhere within this gap and compare the equilibrium populations at the bottom of the two free energy wells for the reactants with minimal influence on the relative pK_a. For instance, changing the value of R_c from 1.3 to 1.5 Å shifts the value of pK_a by less than 0.1 units. Therefore, we conclude that the dependence of the calculated relative pK_a values on the radial cutoff R_c is weak, provided that it has been chosen in the region where the PMF levels off. The extreme insensitivity of the result with respect to the value of R_c is clearly illustrated in Figure 7. It depicts the value of the pK_a calculated from eq 3 assuming as a reference state the top of the barrier in the PMFs, where the constraint force changes sign. We observe an exponentially fast convergence of the pK_a to an essentially fixed value with an increase in the radial cutoff beyond 1.2 Å. We also note that the use of a single cutoff criterion as opposed to two separate ones, R_c(His) and $R_c(H_2O)$, is based on the similarity in the equilibrium bond lengths of the N−H bond in an imidazolium cation (∼1.1 Å) and the O−H bond in a water molecule (∼1.0 Å).

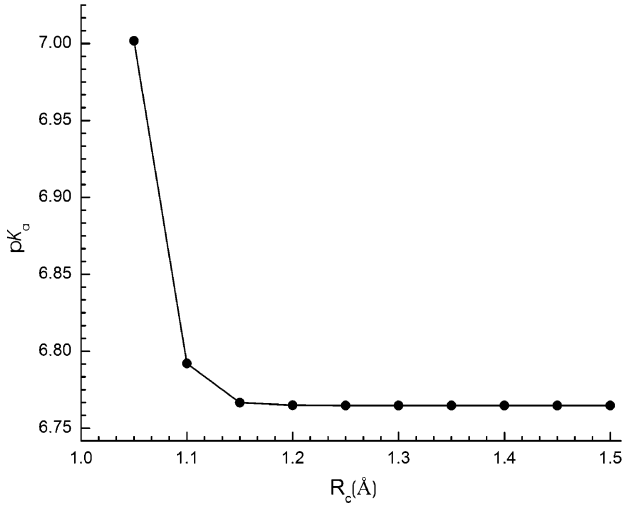

Figure 7. Calculated pK_a value as a function of the radial cutoff R_c.

4. Concluding Remarks

Ab initio molecular dynamics constitutes an attractive method to study solution-phase processes. It automatically includes polarization and finite temperature effects and allows for the study of processes involving bond breaking and formation. It also takes into account the reorganization of the solvent hydrogen bond network during dissociation. This reorganization may play a crucial role in the reaction and is not considered in less expensive quantum mechanical methods based on self-consistent reaction field approaches such as the widely used COSMO or polarizable continuum models.[33−36] In addition to the above advantages it also limits the dependence of the results on empirical parameters. Estimation of pK_a values within the limits of certain approximations is relatively straightforward but computationally expensive. Furthermore, we have shown that the bond conversion process can be monitored and a suitable value for the radial cutoff R_c selected using a number of criteria: structural, dynamical, or electronic. The dependence of the results on the value of R_c is weak, provided that it is chosen after the transition from a covalent to hydrogen bond has occurred. Thus, the more serious limitation appears to be the length of the PMF and the assumption of a reference state at the top of the barrier rather than at the average distance of products in the thermodynamic reference state (C_M of 1 mol L^{-1}). Thus, to make further progress one could consider the extension of the potentials of mean force using multiple constraints.[37,38] One constraint would be used to effect the reactive transformation, and the second (possibly collective) constraint to circumvent the termination of the PMFs due to proton transfer.

Acknowledgment. We thank Dr. Berend Ensing and Dr. Steve O. Nielsen for many helpful discussions. Financial support from the National Science Foundation is gratefully acknowledged. Computer resources were provided, in part, by the Pittsburgh Supercomputing Center through NPACI.

Supporting Information Available: Table of zero point energies and plots of the Mulliken and Löwdin charges and the Mayer bond order as a function of the control parameter ξ. This material is available free of charge via the Internet at http://pubs.acs.org.

References and Notes

(1) Davies, J. E.; Doltsinis, N. L.; Kirby, A. J.; Roussev, C. D.; Sprik, M. *J.* Am. Chem. Soc. **2002**, *124*, 6594−6599.
(2) Li, G. S.; Ruiz-Lopez, M. F.; Maigret, B. *J. Phys. Chem. A* **1997**, *101*, 7885−7892.
(3) Lim, C.; Bashford, D.; Karplus, M. *J. Phys. Chem.* **1991**, *95*, 5610−5620.
(4) Henry, B.; Tekely, P.; Delpuech, J. J. *J. Am. Chem. Soc*. **2002**, *124*, 2025−2034.
(5) Trout, B. L.; Parrinello, M. *Chem. Phys. Lett.* **1998**, *288*, 343−347.
(6) Trout, B. L.; Parrinello, M. *J. Phys. Chem. B* **1999**, *103*, 7340−7345.
(7) Sprik, M. *Chem. Phys.* **2000**, *258*, 139−150.
(8) Car, R.; Parrinello, M. *Phys. Rev. Lett.* **1985**, *55*, 2471−2474.
(9) Silvestrelli, P. L.; Marzari, N.; Vanderbilt, D.; Parrinello, M. *Solid State Commun.* **1998**, *107*, 7−11.
(10) Laria, D.; Kapral, R.; Estrin, D.; Ciccotti, G. *J. Chem. Phys.* **1996**, *104*, 6560−6568.
(11) Hutter, J. et al. *CPMD*, version 3.5; MPI für Festkörperforschung and IBM Research Laboratory: Zurich, Switzerland, 1995−2001.
(12) Boese, A.; Doltsinis, N. L.; Handy, N. C. *J. Chem. Phys.* **2000**, *112*, 1670−1678.
(13) Hamprecht, F. A.; Cohen, A. J.; Tozer, D. J.; Handy, N. C. *J. Chem. Phys.* **1998**, *109*, 6264−6271.
(14) Becke, A. D. *Phys. Rev. A* **1988**, *38*, 3098−3100.
(15) Lee, C.; Yang, W.; Parr, R. C. *Phys. Rev. B* **1988**, *37*, 785−789.
(16) Troullier, N.; Martins, J. L. *Phys. Rev. B* **1991**, *43*, 1993−2006.
(17) Kleinman, L.; Bylander, D. M. *Phys. Rev. Lett.* **1982**, *48*, 1425.
(18) Schwegler, E.; Grossman, J. C.; Gygi, F.; Galli, G. *J. Chem. Phys.* **2004**, *121*, 5400.
(19) Grossman, J. C.; Schwegler, E.; Draeger, E. W.; Gygi, F.; Galli, G. *J. Chem. Phys.* **2004**, *120*, 300.
(20) Tuckerman, M. E.; Parrinello, M. *J. Chem. Phys.***1994**, *101*, 1302.
(21) Martyna, G. J.; Klein, M. L.; Tuckerman, M. *J. Chem. Phys*. **1992**, *97*, 2635.
(22) Ivanov, I.; Klein, M. L. *J. Am. Chem. Soc*. **2002**, *124*, 13380−13381.
(23) Doltsinis, N. L.; Sprik, M. *Phys. Chem. Chem. Phys.* **2003**, *5*, 2612−2618.
(24) Sprik, M.; Ciccotti, G. *J. Chem Phys.* **1998**, *109*, 7737−7744.
(25) Bolhuis, P. G.; Chandler, D.; Dellago, C.; Geissler, P. L. *Annu. Rev. Phys. Chem.* **2002**, *53*, 291−318.
(26) Carter, E. A.; Ciccotti, G.; Hynes, J. T.; Kapral, R. *Chem. Phys. Lett.* **1989**, *156*, 472−477.
(27) Chandler, D. *Introduction to Modern Statistical Mechanics*; Oxford University Press: New York, 1987.
(28) Geissler, P. L.; Dellago, C.; Chandler, D.; Hutter, J.; Parrinello, M. *Science* **2001**, *291*, 2121−2124.
(29) Silvi, B.; Savin, A. *Nature* **1994**, *371*, 683−686.
(30) Becke, A. D.; Edgecombe, K. E. *J. Chem. Phys.* **1990**, *92*, 5397−5403.
(31) Mulliken, R. S. *J. Chem. Phys.* **1955**, *23*, 1833−1840.
(32) Mayer, I. *Chem. Phys. Lett.* **1983**, *97*, 270−274.
(33) Cramer, C. J.; Truhlar, D. G. *Chem. Rev.* **1999**, *99*, 2161.
(34) Miertus, S.; Scrocco, E.; Tomasi, J. *Chem. Phys.* **1981**, *55*, 117.
(35) Klamt, A.; Schüürmann, G. *J. Chem. Soc., Perkin Trans. 2* **1993**, *220*, 799.
(36) Klamt, A. *J. Phys. Chem.* **1995**, *99*, 2224.
(37) Sergi, A.; Ciccotti, G.; Falconi, M.; Desideri, A.; Ferrario, M. *J. Chem. Phys.* **2002**, *116*, 6329−6338.
(38) Den Otter, W. K.; Briels, W. J. *Mol. Phys.* **2000**, *98*, 773−78.